

http://pubs.acs.org/journal/aelccp

Stabilizing Graphite Anode in Electrolytes with Nanoscale Anion Networking for High-Rate Lithium Storage

Yikang Yu, Ijayi Xu, Kaining Duanmu, Vaithiyalingam Shutthanandan, Sungun Wi, Zhenzhen Yang, Yuzi Liu, Xingyi Lyu, Kun Qian, Mangilal Agarwal, Zhengcheng Zhang, Yugang Zhang, Tao Li,* Cong Liu,* Vijayakumar Murugesan,* and Jian Xie*



Cite This: ACS Energy Lett. 2024, 9, 5002-5011



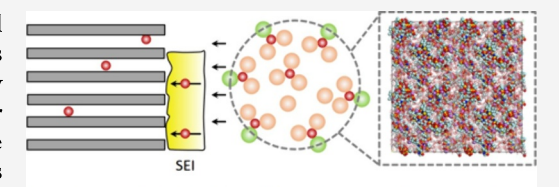
ACCESS

Metrics & More

Article Recommendations

s Supporting Information

ABSTRACT: Graphite is the preferred anode material in commercial lithium-ion batteries (LIBs), but its limited compatibility with various organic molecules restricts the electrolyte solvent options. The primary challenge is solvent co-intercalation with Li ions, leading to graphite layer exfoliation. As a result, electrolyte selection often relies on ethylene carbonate (EC)-based solvents. In this study, we introduce electrolytes featuring a nanoscale anion network ordering that hinders the liquid-phase exfoliation of graphite. This network, formed from concentrated long-chain lithium salts, traps free dioxolane (DOL) molecules, reducing the



Nanostructured electrolyte with anion network traps solvent molecules to mitigate graphite layer exfoliation

interactions between graphite particles and solvents during Li intercalation. Our findings reveal a mechanism that stabilizes graphite in otherwise unstable solvents with concentrated salts like LiTFSI, providing key insights for improving LIB performance by addressing electrolyte limitations on graphite anodes.

lthough the discovery of graphite lithium compounds dates back to nearly half a century ago, the utilization of graphite as an anode for lithium storage was first reported in the early 1980s.^{1,2} Subsequent advancements in graphite anode development ultimately led to the commercial success of lithium-ion batteries (LIBs), which effectively replaced unsafe Li metal anodes in the 1990s. The unique lamellar structure of graphite allows for continuous lithium intercalation, offering a theoretical storage capacity as high as 372 mAh g^{-1} . However, the co-intercalation of various solvent molecules, such as propylene carbonate and ethers, into the graphite layer results in layer exfoliation during Li-ion insertion.⁴⁻⁸ Consequently, the limited solvent compatibility of graphite anodes leaves few choices other than ethylene carbonate (EC)-based organic solvents for commercial LIBs. 9 Nevertheless, the frequently employed EC-based electrolyte is prone to oxidation on the surface of high-nickel cathodes (e.g., LiNi_{0.5}Mn_{0.3}Co_{0.2}O₂), leading to a shortened cycle life and reduced thermal abuse tolerance. This constraint of the electrolyte choice has hindered the effective application of advancements in organic electrolyte chemistry over the past three decades to practical LIBs, particularly those designed for high energy density batteries using high-nickel cathodes. Given that graphite remains the predominant anode material in the market, overcoming this limitation by expanding electrolyte choices for graphite anodes and unlocking solvent compatibility would pave the way for high-performance batteries capable of fast charging and reliable operation at low temperatures.

To address this challenge, prior endeavors involving concentrated electrolytes in various solvents have demonstrated effectiveness in protecting the structural integrity of graphite by forming a stable solid electrolyte interphase (SEI) on this surface. However, subsequent investigations have revealed that the presence of a preformed stable SEI layer on graphite does not necessarily ensure reversible Li-ion insertion/extraction in unstable electrolyte combinations, thereby challenging the SEI prospect in promoting graphite stability. Instead, the local coordination structure of Li ions within the electrolyte has emerged as a more critical factor in determining the graphite stability. Specifically, the formation of certain aggregation states (e.g., aggregated ion pairs) with NO₃⁻ anions has been shown to mitigate the interaction between Li ions and solvents, thereby reducing solvent co-

Received: July 24, 2024
Revised: September 2, 2024
Accepted: September 11, 2024
Published: September 20, 2024





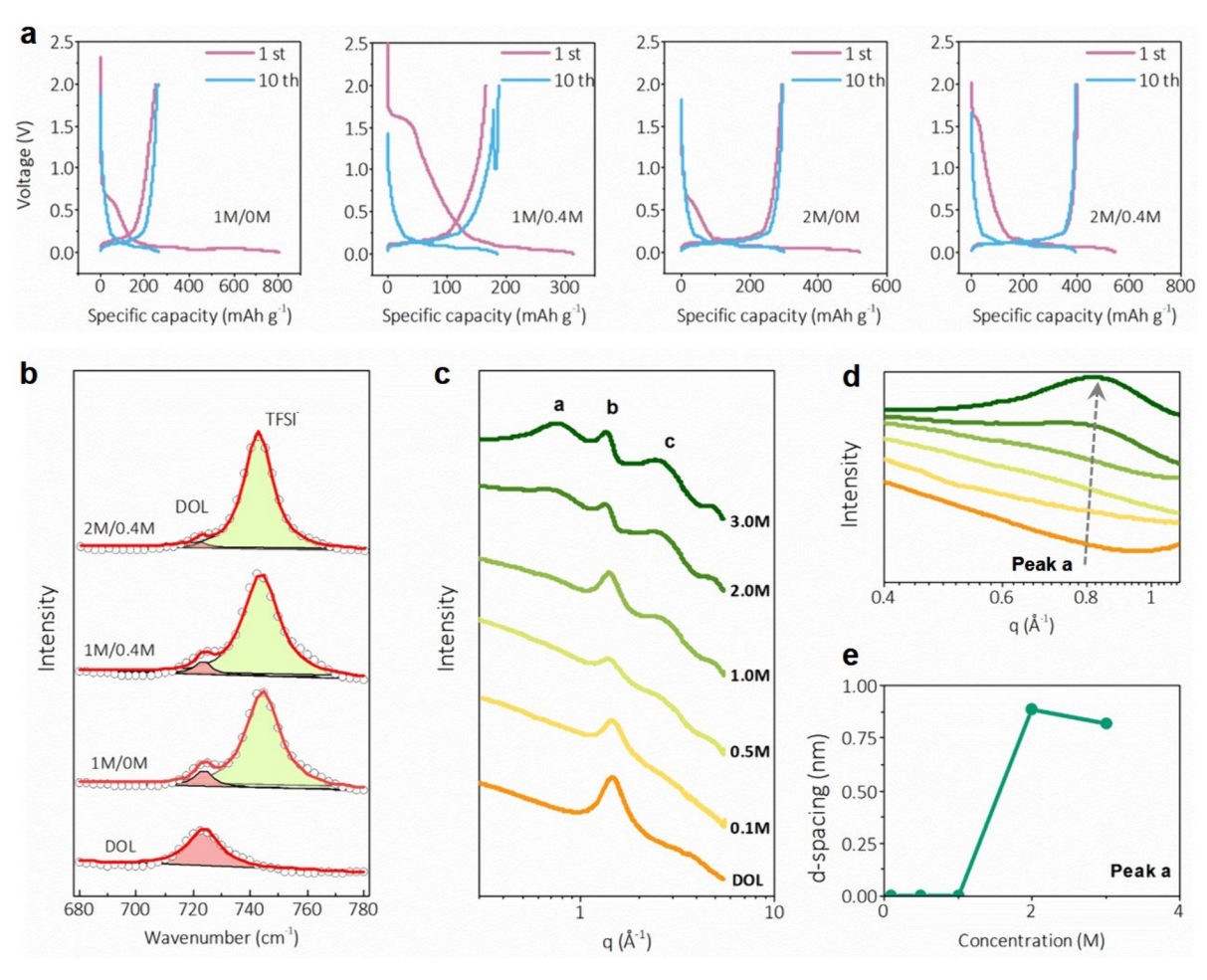


Figure 1. Electrolyte with nanoscale anion network for stabilizing graphite anodes. (a) The 1st and 10th charge and discharge curves (0.1 C) of the graphite anode with different LiTFSI and LiNO₃ concentrations in DOL. (b) Deconvolution of free DOL molecules and S-N-S bending of TFSI⁻ from Raman spectroscopy. (c, d) SAXS patterns acquired with a small q range for pure DOL and LiTFSI containing electrolytes, which reveal the construction of an anion network with increasing LiTFSI concentration. (e) The evolution of the d-spacing of peak a with LiTFSI concentration in the DOL solvent.

intercalation. Nevertheless, the adoption of high concentrations of long-chain lithium salts (e.g., lithium bis-(trifluoromethanesulfonyl)imide and lithium bis-(fluorosulfonyl), LiTFSI and LiFSI), is commonly observed in those unconventional non-EC-based electrolytes for stable graphite anodes in various solvents such as acetonitrile (AC), 14 tetrahydrofuran (THF),15 dimethyl sulfoxide (DMSO),15 sulfone (SL), 15 1,3-dioxolane (DOL), 16,18 1,2-dimethoxyethane (DME), ^{17,18} and phosphate. ¹⁹ The recently proposed theory of Li coordination, however, has struggled to fully explain the enhanced stability of graphite in these concentrated electrolytes with a few additives (e.g., NO₃⁻). Consequently, the critical role of concentrated long-chain anions, particularly TFSI, in enhancing graphite stability has been largely overlooked and requires further attention to reconcile different perspectives on this matter.

In this study, we revisited the stability of graphite anodes by varying the concentrations of long-chain lithium salts (LiTFSI) within a DOL-based electrolyte system. Our findings indicate that increasing the concentrations of LiTFSI (2 M LiTFSI in DOL) facilitates reversible lithium-ion (de)intercalation. Small-angle X-ray scattering analysis (SAXS) reveals an overall charge ordering structure at the nanoscale in this electrolyte, while the absence of significant Raman peak shifts implies that

the local Li coordination structure remains comparable to that of less stable electrolytes with lower LiTFSI concentrations (1 M LiTFSI in DOL). These observations suggest that the overall nanostructure of the electrolyte, dictated by the ordering of long-chain anions, plays a pivotal role in enhancing graphite stability rather than the local Li coordination structure at the atomic scale. Given the prevalence of this charge ordering structure in concentrated electrolytes containing longchain lithium salts, 21,22 our results may extend to other reported unconventional electrolytes that stabilize graphite anodes. 14-19 Furthermore, the addition of LiNO₃ (0.4 M) promotes the formation of a fluorinated SEI layer, which enhances the lithium kinetics. Consequently, we have demonstrated a nanostructured electrolyte with an anion network (2 M LiTFSI/0.4 M LiNO3 in DOL) with significantly improved Li-ion kinetics for graphite anodes, achieving a theoretical capacity of graphite at room temperature (\sim 370 mAh g⁻¹). The specific capacity of graphite cycled in this nanostructured electrolyte (>200 mAh g⁻¹) is about seven times that of graphite electrodes cycled in traditional EC-based electrolytes (<30 mAh g⁻¹) at a 2 C rate.

The stability of the graphite anode was systematically investigated in a DOL-based electrolyte containing different concentrations of long-chain LiTFSI salts and LiNO₃ additives.

ACS Energy Letters http://pubs.acs.org/journal/aelccp Letter

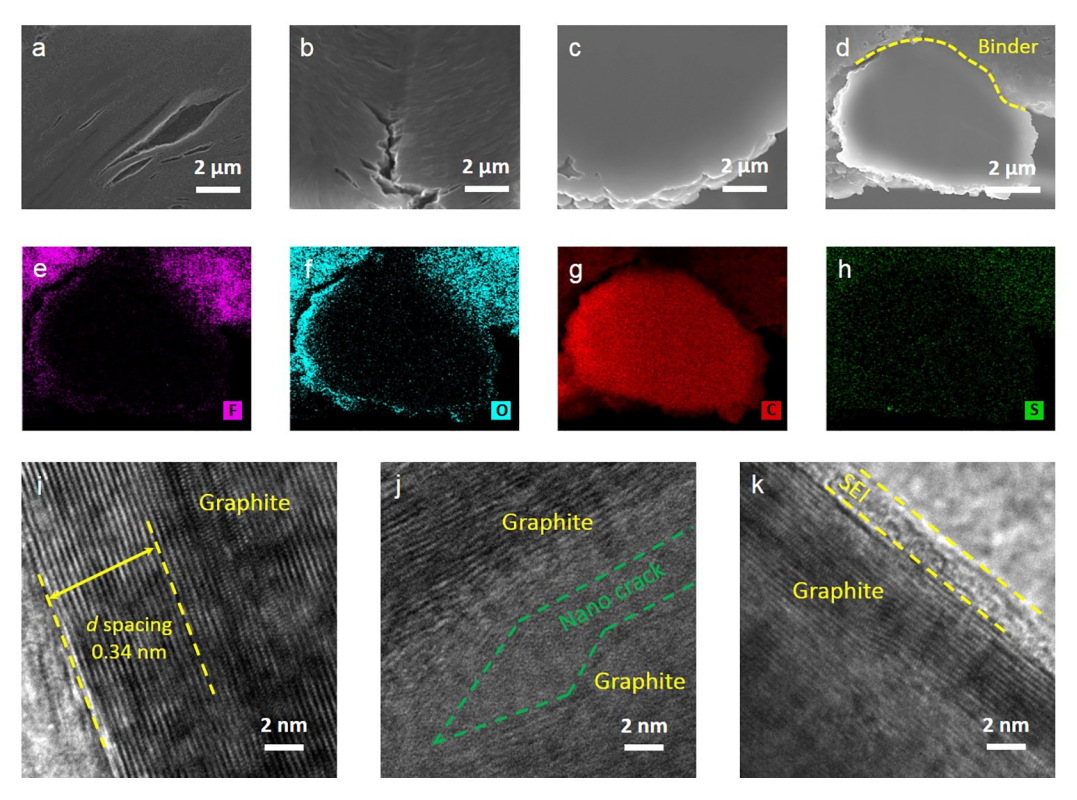


Figure 2. Visualization of solvent co-intercalation-induced graphite inner exfoliation. CS-SEM images of inner graphite structures after 10 cycles in DOL-based electrolytes: (a) 1 M LiTFSI in DOL, (b) 1 M LiTFSI/0.4 M LiNO₃ in DOL, and (c) 2 M LiTFSI/0.4 M LiNO₃ in DOL. (d) Single particle imaging of graphite cycled in electrolyte of 2 M LiTFSI/0.4 M LiNO₃ in DOL and (e—h) related EDS mapping results. (i—k) TEM images of graphite cycled in electrolyte of 2 M LiTFSI/0.4 M LiNO₃ in DOL show the (i) graphite layer structure, (j) inner nanoscale crack, and (k) SEI layer.

Electrolytes with a 2 M concentration of LiTFSI exhibit a typical charge-discharge curve, showcasing a specific capacity exceeding 300 mAh g⁻¹ at 0.1 C, indicative of reversible Li intercalation and extraction at this elevated concentration (Figure 1a). In contrast, an abnormally large initial Li intercalation specific capacity (>800 mAh g⁻¹) is observed in the electrolyte with 1 M LiTFSI, widely considered a consequence of Li⁺—solvent co-intercalation.^{23,24} Subsequent cycling reveals a limited specific capacity (<200 mAh g⁻¹, 10th cycle), possibly due to the failure of the graphite inner structure resulting from this co-intercalation. The addition of LiNO₃ additives to these electrolytes shows stability similar to that of the corresponding LiNO₃-free electrolyte (Figure 1a). To deepen our understanding of graphite stability in these electrolytes and the underlying mechanisms, Raman spectroscopy was employed to probe the Li coordination structures. Two characteristic peaks at 722 and 746 cm⁻¹, corresponding to the O-C-O bending mode of DOL molecules and S-N-S bending of TFSI ions (Figure 1b), respectively, 25,26 were detected in these Li salt containing electrolytes. With an increase in the concentration of LiTFSI, the relative peak intensity of DOL solvent (722 cm⁻¹) significantly weakened compared to the TFSI⁻ intensity (746 cm⁻¹). The negligible TFSI Raman peak shift (S-N-S bending) in these electrolytes suggests a similar Li coordination structure at the atomic level. However, despite having a comparable Li coordination structure to the 2 M concentration electrolyte, the charge and discharge curves (Figure 1a) indicate solvent co-intercalation and a degraded Li storage performance of the graphite anode cycled in the 1 M LiTFSI electrolyte. These observations strongly suggest that the local Li coordination

structure alone is insufficient to account for the graphite stability observed in this DOL-based electrolyte system.

To comprehensively explore electrolyte nanostructures beyond atomic solvation binding, small-angle X-ray scattering (SAXS) was employed to detect the short-range order arising from interactions between adjacent ions and solvent molecules. 21,27 As illustrated in Figure 1c, three distinct peaks, labeled as peak a, peak b, and peak c, were identified in these DOL-based electrolytes. These peaks correspond to anion network structures, DOL molecules, and the neighboring atoms of either the same anion or adjacent anions based on our previous investigations. ^{28–31} As the LiTFSI concentration gradually increased, peak a gradually become more prominent and shift to a higher q (Figure 1d), indicating a reduction in the average distance between TFSI (Figure 1e). As a result, peak a represents the anion network structure with those closely packed long-chain TFSI⁻ anions. The corresponding *d*spacing was calculated using $d = 2\pi/q$, and its relationship with concentration is shown in Figure 1e. An ordered anion solvation nanostructure is constructed through Li-ion coordination at a relatively high LiTFSI concentration (2 to 3 M) with a d-spacing of ~ 0.8 nm. Furthermore, the addition of LiNO₃ into these electrolytes does not change the anion network and corresponding d-spacing, suggesting the key role of LiTFSI concentration in the electrolyte nanostructures (Figure S1). Moreover, the stable cycling of graphite anodes in a 3 M LiTFSI DOL electrolyte (Figure S2) further confirms that the gradually constructed anion network at the nanoscale is highly relevant to the suppression of solvent co-intercalation.

The stability of graphite in the nanostructured electrolyte (2 M LiTFSI/0.4 M LiNO₃ in DOL, hereinafter referred to for

ACS Energy Letters http://pubs.acs.org/journal/aelccp Letter

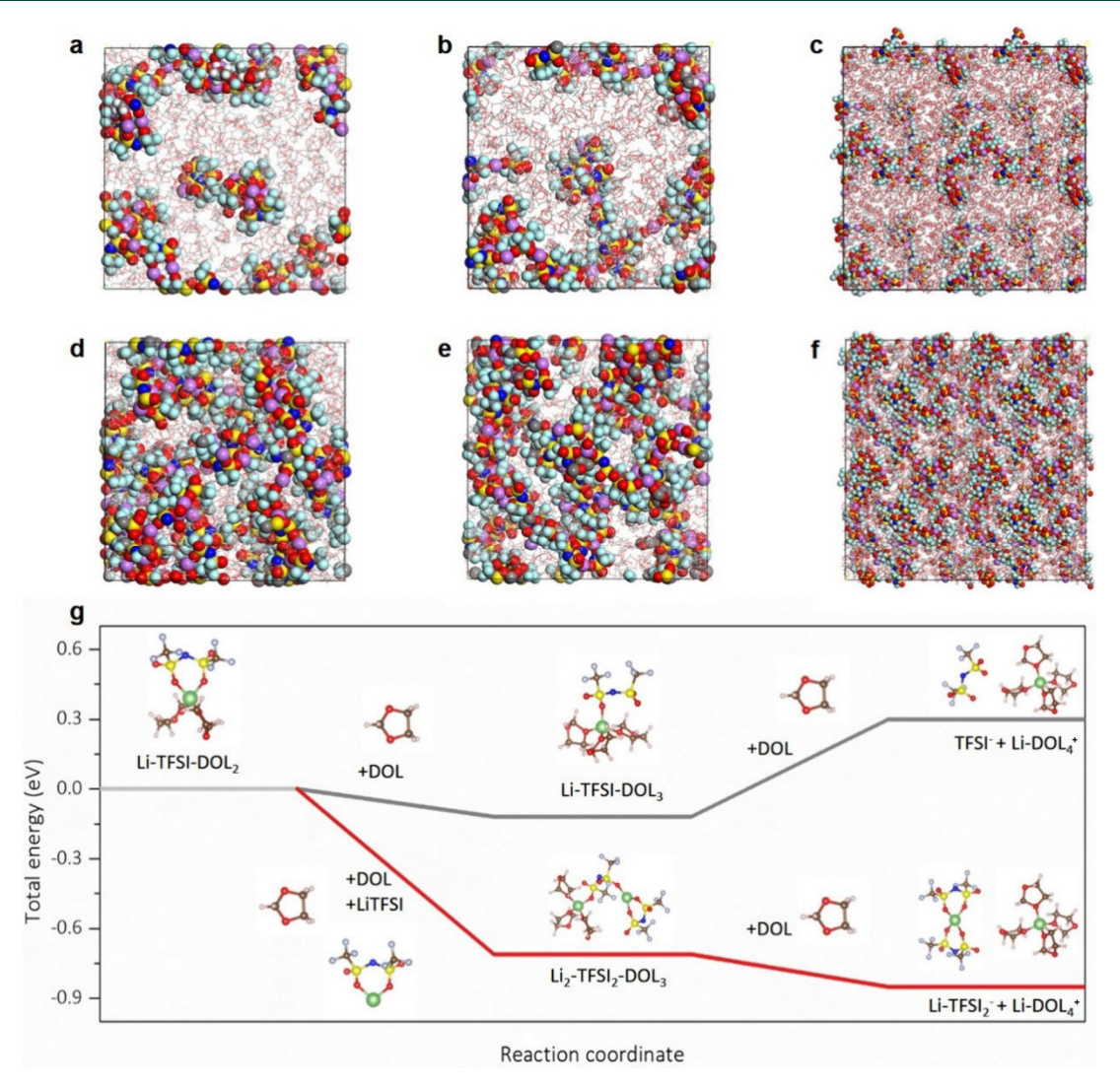


Figure 3. (a–f) MD simulations of electrolyte structures in DOL-based electrolyte and (g) reaction energy profile and molecular models of reaction intermediates of stripping of TFSI $^-$ anion from Li ions, which is evaluated by the formation of a solvent-separated ion pair (SSIP, Li-DOL $_2$ $^+$) from a contact ion pair (CIP, Li-TFSI-DOL $_2$). MD snapshots of 1 M LiTFSI in DOL with (a) 1 ns, (b) 1.5 ns, and (c) related electrolyte structure revealed in an enlarged 2 \times 2 super cell. MD snapshots of 2 M LiTFSI in DOL with (d) 1 ns, (e) 1.5 ns, and (f) related electrolyte nanoscale anion network structure in an enlarged 2 \times 2 super cell. Note the line style represents the DOL molecules, and CPK style represents the LiTFSI. Color code (a–f): purple, Li; gray, C; red, O; blue, N; yellow, S; white, H; cyan, F. Color code (g): red, O; blue, N; yellow, S; green, Li; brown, C; gray, F; white, H.

subsequent discussions) was further scrutinized using ex situ X-ray diffraction (XRD) and scanning electron microscopy (SEM) post cycling. The characteristic peaks of the graphite layer structure (002) remained consistent after cycles, exhibiting no shifts compared to the pristine graphite electrode (Figure S3). Additionally, complete graphite particles maintained similar morphologies to those cycled in EC-based electrolytes (Figure S4). These results signify the preserved crystal structure integrity of the graphite particles cycled in the nanostructured electrolyte. To visualize the impact of graphite exfoliation on the inner structure of cycled graphite electrodes, cross-sectional scanning electron microscopy (CS-SEM) and high-resolution transmission electron microscopy (TEM) were employed. Severe inner cracks were observed in graphite cycled in 1 M LiTFSI (Figure 2a, Figure S5a-c) and 1 M LiTFSI/0.4 M LiNO₃ (Figure 2b, Figure S 5d-f) electrolytes, aligning with their charge-discharge curve behavior (Figure 1a). These cracks are attributed to graphene layer exfoliation of graphite particles caused by large solvent molecule co-

intercalation.³² Despite structural failure after cycles, the nanostructured electrolyte demonstrated an intact inner structure (Figure 2c,d, Figure S5g-i), suggesting reversible Li uptake and extraction. Energy dispersive X-ray spectroscopy (EDS) was utilized to analyze the elemental distribution in the cross section of a single graphite particle, revealing uniform carbon element distributions corresponding to the graphite structure (Figure 2g, Figure S6). External elements such as fluorine and oxygen from the formation of the solid electrolyte interphase (SEI) after cycles were observed on the particle surface (Figure 2e,f, Figure S6). Interestingly, the addition of LiNO₂ leads to a transformation from an outer layer distribution (Figure S6d) to a random distribution of sulfur throughout the entire particle (Figure 2h, Figure S6i). This different sulfur distribution can be explained by the degree of sulfur decomposition from the LiTFSI (S source). The LiNO₃ is easily decomposed at a quite high voltage (~1.5 V vs Li/ Li⁺),³³ and the formed SEI components from LiNO₃ mitigate further sulfur decomposition on the graphite surface due to the

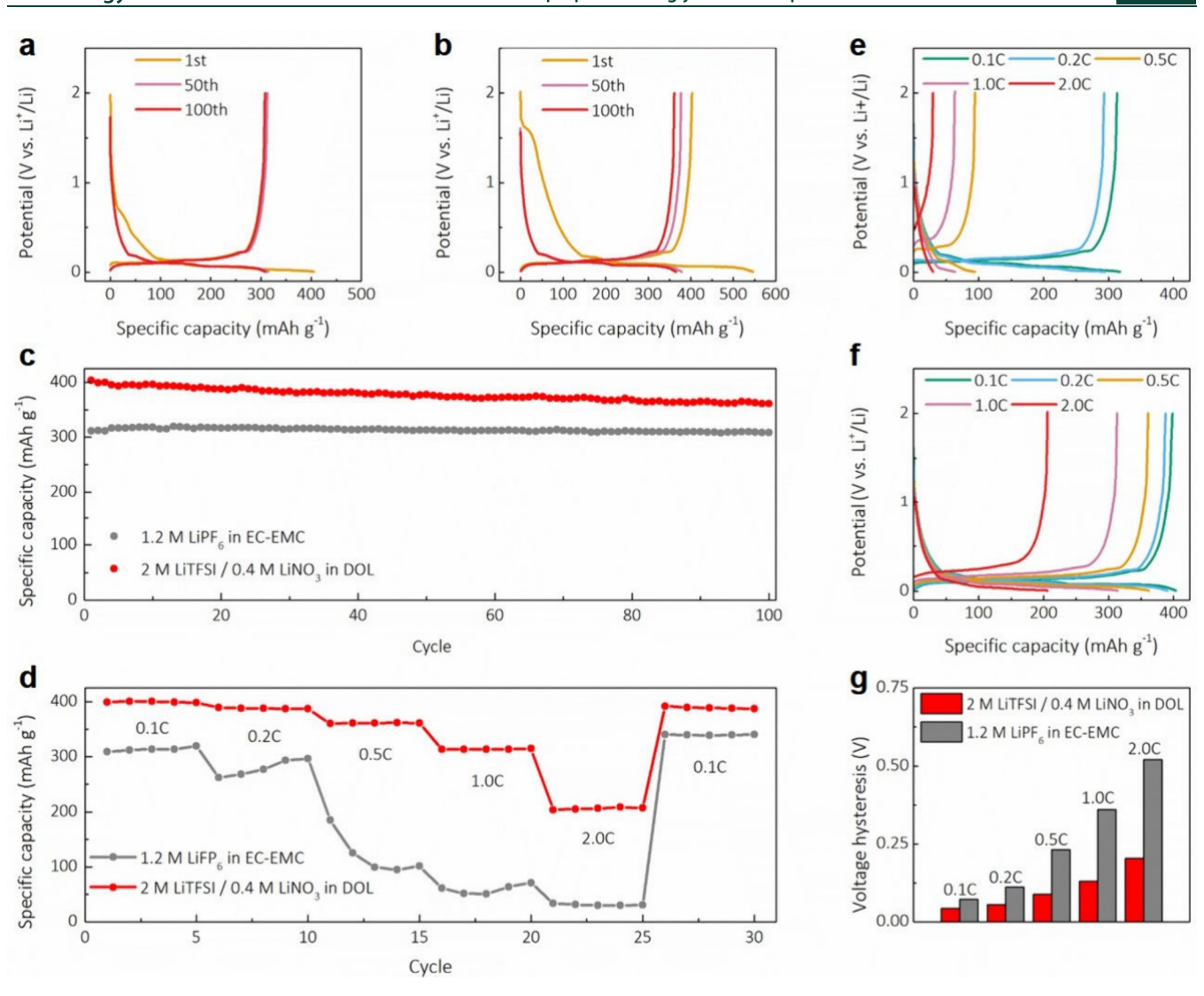


Figure 4. Electrochemical performance of graphite anode in a traditional EC-based electrolyte and nanostructured electrolyte. Typical charge—discharge curves (0.1 C) of graphite electrode in 1.2 M LiPF₆ in (a) EC-EMC electrolyte and (b) 2 M LiTFSI/0.4 M LiNO₃ in DOL electrolyte. (c) Cycling stability (0.1 C) and (d) rate performance of graphite electrode in EC-based electrolyte and nanostructured electrolyte. Charge—discharge curves of graphite electrode at different C rates in different electrolytes: (e) EC-based electrolyte and (f) nanostructured electrolyte. (g) The voltage hysteresis at various C rates based on the difference between the average charge—discharge voltage.

electron insulation nature of the formed SEI layer. Consequently, a much lower S concentration on the graphite surface is revealed in LiNO₃-added electrolytes (see Figure S7 for a more detailed discussion). After 10 cycles in our nanostructured electrolyte, transmission electron microscopy (TEM) images revealed a surface layer approximately 2 nm in thickness covering the graphite layer structure, consistent with the SEI structure resulting from electrolyte decomposition (Figure 2k). Despite the retained structural integrity observed in the SEM images (Figure 2c,d, Figure S5g-i), a few nanoscale cracks (Figure 2j) were identified in the TEM images, indicating limited graphite exfoliation at the nanoscale due to the formation of the anion network, in contrast to the microsized cracks observed in unstable electrolytes (Figure 2a,b).

The liquid-phase exfoliation of graphite, often described as a fragmentation mechanism, involves a rupture process triggered by external forces such as ultrasound-induced cavitation, among others. Additionally, graphite can be exfoliated

directly in various organic solvents through a process resembling quasi-dissolving. 37,38 Organic solvents with surface tensions or energies similar to those of graphene can effectively exfoliate graphite into graphene spontaneously. 39,40 During the lithium-ion intercalation process, driven by the potential difference between the anode and cathode, the friction between the diffusing lithium ions and free solvent molecules acts as an external force, intensifying the exfoliation of graphite into graphene. In the electrolyte, two types of solvent molecules coexist: those bound with lithium ions (termed bound solvent molecules) and free solvent molecules with minimal interactions with lithium ions. In DOL-based electrolytes, the exfoliation of graphite is predominantly induced by the free solvent molecules rather than the bound solvent molecules with lithium ions (see Supplementary Note 1 for detailed discussions). The confinement of free DOL molecules within the anion network is advantageous, as it weakens the interaction between graphite and these free molecules, thereby suppressing graphite exfoliation. To explore this phenomenon further, a SAXS combined molecular dynamics (MD) simulation of two electrolyte systems (1 M LiTFSI and 2 M LiTFSI in DOL) was performed, which represents the structural transition point of the nanoscale anion network formation (peak b, Figure 1c,d). Figure 3a—c illustrates the local arrangement of anions in which stacking individually forms clusters at a relatively low LiTFSI concentration (1 M). In contrast, the increase of LiTFSI concentration to 2 M leads to a formation of an overall anion network (Figure 3d—f), which confines the DOL molecules inside this network. Such confinement of free DOL molecules potentially reduces the interaction between graphite and solvent molecules, and thus, the DOL co-intercalation into the graphite layer is suppressed during lithium intercalation.

On the other hand, as Li ions intercalate, solvated Li ions in the electrolyte must remove the paired solvent molecules and anions (i.e., TFSI-) to traverse the established SEI layer (Figure 2k). 41 However, removing these paired anions requires significantly more energy compared to removing bound solvent molecules. 42 To understand the energetics induced by the Li intercalation process, computational modeling using density functional theory (DFT) was performed to investigate the energy barrier of removing paired TFSI- with Li ions. A reaction energy profile was constructed to reveal the reaction pathway for the formation of a solvent-separated ion pair (SSIP, Li-DOL₄⁺) by removing paired anions from a typical contact ion pair (CIP, Li-TFSI-DOL₂). As shown in Figure 3g, when DOL breaks one of the O-Li bonds between TFSI and Li⁺, forming a Li-TFSI-DOL₃ with a dangling O (gray line), the reaction is exothermic by -0.12 eV. However, when adding a second DOL molecule to form a TFSI and a Li-DOL₄⁺, the reaction becomes endothermic by 0.30 eV. This could correspond to the electrolytes with low concentrations of LiTFSI, where the dangling O from Li-TFSI-DOL₃ and TFSI⁻ in the final structure are not well stabilized, making the overall thermodynamics endothermic. In contrast, with a higher concentration of LiTFSI, there is an interaction between the initial state, Li-TSFI-DOL₂, and a second Li-TSFI complex, as indicated by the red line. When adding DOL to Li-TFSI-DOL₂, in the electrolyte with a higher concentration of LiTFSI, the dangling O from Li-TFSI-DOL3 can be stabilized by the Li⁺ from a secondary Li-TFSI, where the reaction potential energy is exothermic by -0.71 eV (red line). Adding a second DOL to Li₂-TFSI₂-DOL₃, the complex decomposes to Li-DOL₄⁺ and Li-TFSI₂⁻ ions, and this step is also exothermic by -0.14 eV. When considering the entropic effect and evaluating the free energy, a similar trend is also observed (Figure S18). Therefore, these two pathways explicitly show that with higher LiTFSI concentration, the formation of Li-DOL₄⁺ by removing paired anions is thermodynamically favored due to better TFSI- stabilization by a nearby LiTFSI. In contrast, in electrolytes with low LiTFSI concentration, this process is thermodynamically not favored. This finding suggests that an electrolyte with a higher LiTFSI concentration, featuring a thermodynamically favored anion stripping process, may result in a lower energy barrier for the lithium intercalation process, further reducing interactions between diffused lithium ions and free solvent molecules, thereby enhancing graphite stability.

An intriguing phenomenon that captured our attention is the stable specific capacity exceeding the theoretical capacity of graphite (\sim 390 mAh g⁻¹) observed in the nanostructured electrolyte with LiNO₃ additives (0.4 M) (Figure 1a). Given

this intriguing finding, we further investigated the capacity contribution from Super P (SP) conductive carbon black. Carbon materials can store charge through various mechanisms, such as faradaic intercalation, capacitive, and pseudocapacitive charge storage. 43,44 To evaluate the SP capacity contribution to the graphite anode, electrodes composed of pure SP and poly(vinylidene difluoride) (PVDF) as a binder (9:1, by mass) were fabricated. Similar capacities were revealed for SP in both EC-based and nanostructured electrolytes (~160 mAh g⁻¹) (Figure S9). After the SP capacity contribution was subtracted, a theoretical capacity of graphite (~370 mAh g⁻¹) was approached in our nanostructured electrolyte at room temperature. To the best of our knowledge, previously reported graphite electrodes with the best capacity achieved being as high as \sim 370 mAh g⁻¹ (0.1 C, room temperature) had not subtracted the additives' capacity contribution (e.g., Fe₃O₄, SP).⁴⁵

Further exploration of the electrochemical performance of graphite in the nanostructured electrolyte was systematically studied compared with that in the traditional EC-based electrolyte, as presented in Figure 4. The graphite electrode was cycled between 0.005 and 2.0 V (vs Li+/Li) at different C rates in both electrolytes at room temperature. A typical charge-discharge curve at 0.1 C is demonstrated in the nanostructured electrolyte (Figure 4b) and is similar to that of the EC-based electrolyte (Figure 4a), suggesting reversible lithium intercalation and extraction (Figure 4c). The slightly larger capacity decay in the nanostructured electrolyte is able to be explained by the nanoscale cracks, as observed from the TEM image (Figure 2j). These observations suggest that the exfoliation of graphite at a smaller scale persists, contributing a smaller average Coulombic efficiency (Figure S10) of graphite within the nanostructured electrolyte (99.34%) compared to that within the EC-based electrolyte (99.41%). Long-term cycling at 0.2 C for up to 200 cycles (Figure S11) further validated the stable Li-ion intercalation and extraction behaviors in our nanostructured electrolyte. The rate-capability test shows that the graphite electrodes maintain their performance at elevated charge-discharge rates of up to 2 C (Figure 4d) in the nanostructured electrolyte. Up to a rate of 0.2 C, both electrodes in the EC-based electrolyte and nanostructured electrolyte demonstrate a similar voltage profile with inconspicuous voltage hysteresis (Figure 4e,f), defined as the difference between the average charge and discharge voltage. At such low rates, the Li insertion and extraction kinetics limitation is negligible, leading to a close specific capacity in both electrolytes. However, raising the cycling rate to 0.5 C reveals a significant difference between these two electrolytes, not only in voltage profiles but also in specific capacity. At a high C rate $(\geq 0.5 \text{ C})$, a more desirable potential plateau and a much smaller voltage hysteresis (Figure 4g) are obtained in the nanostructured electrolyte. Moreover, the specific capacity of graphite cycled in the nanostructured electrolyte is about seven times that of graphite electrodes cycled in the traditional EC-based electrolyte at a 2 C rate. The electrochemical window limit of the nanostructured electrolyte was examined by linear sweep voltammetry (LSV) tests in a Li-Al cell, which shows that our nanostructured electrolyte can be stable at a voltage as high as 4.4 V (Figure S12). A further increase of LiTFSI concentration from 2 to 3 M is able to elevate the stable voltage to 4.5 V, which can be used in most of the cathode materials. Based on the LSV results, we performed a galvanostatic cycling performance test using

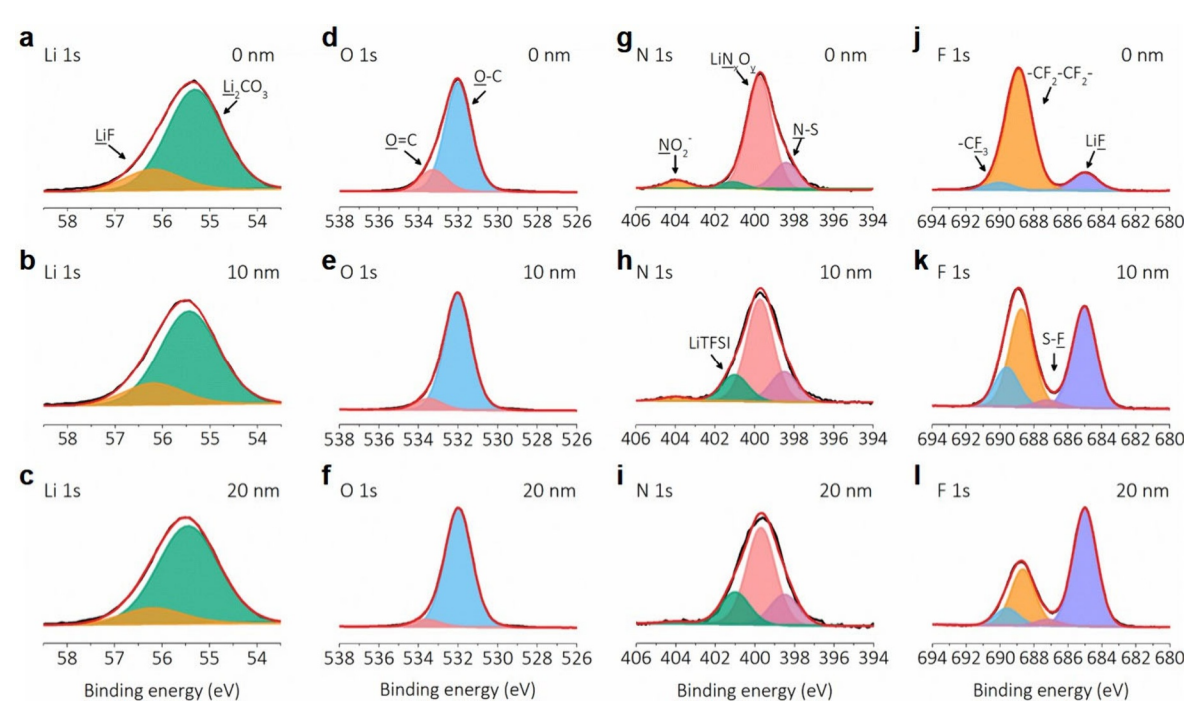


Figure 5. Characterization of SEI components on a cycled graphite electrode by XPS. XPS spectra of (a-c) Li 1s, (d-f) O 1s, (g-i) N 1s, and (j-l) F 1s for a graphite electrode after 10 cycles in electrolyte of 2 M LiTFSI/0.4 M LiNO₃ in DOL (0.1 C) with different depths as indicated: 0, 10, and 20 nm indicate the depths at which the spectra were acquired.

LiNi $_{0.8}$ Co $_{0.1}$ Mn $_{0.1}$ O $_2$ (NCM811) in our nanostructured electrolyte. Facile oxidation of the conventional EC-based electrolyte on the surface of high-nickel cathodes has been widely discovered. As a result, NCM811 suffers from a sudden capacity loss after ~170 cycles at 0.5 C (Figure S13a), resulting in a low capacity retention (~21.5%, Figure S13b) after 300 cycles. However, by eliminating the EC in our DOL electrolyte, the NCM811 demonstrates a superior cycling stability with a capacity retention of ~93.0% after 300 cycles at 0.5 C (Figure S13c). These results further suggest the importance of unlocking the electrolyte limitation on graphite anodes to avoid a EC-based conventional electrolyte for high energy density LIBs.

Compared to the LiNO₃-free nanostructured electrolyte (2 M LiTFSI in DOL), the addition of LiNO₃ into the electrolyte contributes to improved electrochemical performance (Figure 1a), possibly stemming from the formation of a fluorinated solid electrolyte interface (SEI) with fast lithium conduction. 46,47 In addition to the SEI structure study from electron microscopy techniques (Figure 2e-h), X-ray photoelectron spectroscopy (XPS) was further applied to probe the components of the SEI layer on the cycled graphite electrode at different depths (0, 10, and 20 nm). For the graphite cycled in DOL-based electrolytes, SEI layer components consisting of inorganic species (e.g., Li₂CO₃, LiF, LiOH) and organic species (e.g., C-C, C-O, RLi, etc.) have been detected (Figure 5, Figures S14-S16). The most significant difference among these electrolytes lies in their fluorine compound content (LiF) and LiN_xO_y species (~400 eV in Figure 5g-i). With the addition of LiNO3 into the DOL electrolyte system, the intensity of LiF (Figure 5j-l, Figure S15j-l) and LiN, O, peaks (Figure 5g-i, Figure S15g-i) has been greatly enhanced compared with the single LiTFSI system (1 M LiTFSI in DOL, Figure S14g-l). The combination of LiF/LiN, O, has been widely discovered as the SEI components in LiNO₃-added

electrolytes. 33,48,49 It has been discovered that the NO₃⁻ is able to enhance the interaction between TFSI- and Li+, promoting the decomposition of TFSI and contributing to the formation of a fluorinated SEI. 50 Such results have been further confirmed by corresponding element contents, where a lower F concentration has been found in the single LiTFSI electrolyte (~1%, Figure S16d). F-rich SEI structures (>10%, Figure S16h-l) in these LiNO₃-added systems suggest a full fluorine decomposition of LiTFSI on the graphite surface. In contrast, much lower S element concentrations (1.5-2% vs ~6% in 1 M LiTFSI in DOL) are detected, which is consistent with the energy dispersive X-ray spectroscopy (EDS) results showing outer layer S distribution in the graphite cycled in 1 M LiTFSI in DOL (Figure S16d). Graphite cycled in 1 M LiTFSI/0.4 M LiNO₃ and 2 M LiTFSI/0.4 M LiNO₃ exhibit similar SEI components, while the addition of LiNO₃ significantly changes their SEI structures. The cooperation between LiNO₃ and LiTFSI results in high LiF (Figure 5j-l) and LiN_xO_y (Figure 5g-i) content from a new decomposition pathway, as indicated by cyclic voltammetry and LSV curves (Figure S17). The contributed fluorinated SEI is believed to dictate the physicochemical properties, such as the interfacial energy, Li-ion diffusion behaviors, mechanical stability, and so on. 51 However, at a slightly lower concentration, a similar SEI structure (1 M LiTFSI/0.4 M LiNO₃) fails to deliver smooth lithium (de)intercalation as the nanostructured electrolyte (2 M LiTFSI/0.4 M LiNO₃), further suggesting that the role of the SEI on the graphite stability has been overemphasized.¹⁴ On the other hand, fluorides largely reduce the activation energy barrier for Li-ion diffusion across the SEI, resulting in fast Li diffusion. 52-54

In summary, our study revisited the stability of graphite during lithium-ion (de)intercalation, critically examining the conventional viewpoint of liquid graphite exfoliation. We propose that increasing the concentration of long-chain LiTFSI

salt leads to the formation of an overall charge ordering electrolyte nanostructure with an anion network, as revealed by SAXS and MD simulations. The resulting anion network effectively confines free DOL solvent molecules, mitigating the interaction between graphite particles and free solvent molecules during Li (de)intercalation. Our findings extend beyond this specific electrolyte composition, as the observed electrolyte charge ordering nanostructure is universal in high concentration electrolytes with long-chain lithium salts (LiTFSI). 21,22,55 Consequently, our results offer an explanation for the superior stability of graphite reported in high LiTFSI concentration electrolytes with various unusual solvents. 14-19 Furthermore, the addition of LiNO3 to the nanostructured electrolyte contributes to the formation of a fluorinated SEI, enhancing the Li intercalation kinetics. As a result, our nanostructured electrolyte exhibits a theoretical capacity of graphite (\sim 370 mAh g⁻¹, 0.1 C) and significantly improved the fast-charging capability, demonstrating reversible lithium insertion and extraction. From our studies, it is demonstrated that the stability of the graphite is determined by the nanostructure of the electrolyte, while the SEI affects the kinetics of lithium-ion (de)intercalation to a great extent. In conclusion, our results provide a nuanced understanding of the mechanism governing graphite stability in relation to electrolyte nanostructure, challenging the widely accepted standpoint based solely on the SEI or Li coordination structure.

ASSOCIATED CONTENT

Supporting Information

The Supporting Information is available free of charge at https://pubs.acs.org/doi/10.1021/acsenergylett.4c02011.

Experimental details and computational methods, additional electrochemical information, SEM images of the exfoliated graphite, and XPS characterization (PDF)

AUTHOR INFORMATION

Corresponding Authors

Tao Li — Department of Chemistry and Biochemistry, Northern Illinois University, Dekalb, Illinois 60115, United States; X-ray Science Division, Advanced Photon Source, Argonne National Laboratory, Lemont, Illinois 60439, United States; ○ orcid.org/0000-0002-4913-4486; Email: taoli@anl.gov

Cong Liu — Chemical Sciences and Engineering Division, Argonne National Laboratory, Lemont, Illinois 60439, United States; orcid.org/0000-0002-2145-5034; Email: congliu@anl.gov

Vijayakumar Murugesan — Physical and Computational Sciences Directorate, Pacific Northwest National Laboratory, Richland, Washington 99352, United States; ⊚ orcid.org/ 0000-0001-6149-1702; Email: vijay@pnnl.gov

Jian Xie — School of Mechanical Engineering, Purdue University, West Lafayette, Indiana 47907, United States; orcid.org/0000-0002-9800-0206; Email: jxie@purdue.edu

Authors

Yikang Yu — School of Mechanical Engineering, Purdue University, West Lafayette, Indiana 47907, United States; orcid.org/0000-0002-6101-2393

- Jiayi Xu Chemical Sciences and Engineering Division, Argonne National Laboratory, Lemont, Illinois 60439, United States; ◎ orcid.org/0000-0003-1763-6251
- Kaining Duanmu Physical and Computational Sciences Directorate, Pacific Northwest National Laboratory, Richland, Washington 99352, United States; ○ orcid.org/ 0000-0002-9865-8710
- Vaithiyalingam Shutthanandan Physical and Computational Sciences Directorate, Pacific Northwest National Laboratory, Richland, Washington 99352, United States; Oorcid.org/0000-0003-2957-7535
- Sungun Wi Physical and Computational Sciences Directorate, Pacific Northwest National Laboratory, Richland, Washington 99352, United States
- Zhenzhen Yang Chemical Sciences and Engineering Division, Argonne National Laboratory, Lemont, Illinois 60439, United States; oorcid.org/0000-0002-1073-3799
- Yuzi Liu Center for Nanoscale Materials, Argonne National Laboratory, Lemont, Illinois 60439, United States;
 orcid.org/0000-0002-8733-1683
- Xingyi Lyu − Department of Chemistry and Biochemistry, Northern Illinois University, Dekalb, Illinois 60115, United States; © orcid.org/0000-0002-5781-2486
- Kun Qian Department of Chemistry and Biochemistry, Northern Illinois University, Dekalb, Illinois 60115, United States
- Mangilal Agarwal Department of Biomedical Engineering and Integrated Nanosystems Development Institute, Indiana University Indianapolis, Indianapolis, Indiana 46202, United States; Occid.org/0000-0003-3039-0073
- Zhengcheng Zhang Chemical Sciences and Engineering Division, Argonne National Laboratory, Lemont, Illinois 60439, United States; Oorcid.org/0000-0002-0467-5801
- Yugang Zhang Center for Functional Nanomaterials, Brookhaven National Laboratory, Upton, New York 11973, United States

Complete contact information is available at: https://pubs.acs.org/10.1021/acsenergylett.4c02011

Author Contributions

"Y.Y. and J.X. (Jiayi Xu) contributed equally to this work. Y.Y. and J.X. (Jian Xie) proposed this research and designed the experiments. Y.Y. performed the electrochemical measurements and conducted the XRD tests. J.X., K.D., C.L., and V.M. performed the DFT calculations. J.X. (Jiayi Xu) and C.L. performed MD simulations. V.S. and S.W. carried out the XPS experiments. The SEM, CS-SEM, and TEM images were acquired by M.A., Z.Y., and Y.L., respectively. SAXS data were obtained and analyzed by X.L., K.Q., Y.Z., and T.L. Y.Y. and J.X. (Jian Xie) prepared the manuscript with discussions and contributions from all authors.

Notes

The authors declare no competing financial interest.

ACKNOWLEDGMENTS

The authors gratefully acknowledge the help from the Post Test Facility at Argonne National Laboratory, supported by the U.S. DOE Vehicle Technologies Office and use of the Advanced Photo Source and Center for Nanoscale Materials, a U.S. Department of Energy Office of Science User Facility, as supported by the U.S. DOE, Office of Basic Energy Sciences, both under Contract No. DE-AC02-06CH11357. This

research used resources of the Center for Functional Nanomaterials and the SMI beamline (12-ID) of the National Synchrotron Light Source II, both supported by U.S. DOE Office of Science Facilities at Brookhaven National Laboratory under Contract No. DE-SC0012704. T.L. is thankful for the support from the U.S. National Science Foundation (Grant No. 2208972 and 2323117). The DFT calculations are done utilizing computational resources provided by the Laboratory Computing Research Center (LCRC) at the Argonne National Laboratory.

REFERENCES

- (1) Guerard, D.; Herold, A. Intercalation of lithium into graphite and other carbons. *Carbon* 1975, 13 (4), 337–345.
- (2) Yazami, R.; Touzain, P. A reversible graphite-lithium negative electrode for electrochemical generators. *J. Power Sources* **1983**, 9 (3), 365–371.
- (3) Dahn, J. R. Phase diagram of LixC6. Phys. Rev. B Condens Matter 1991, 44 (17), 9170-9177.
- (4) Kim, H.; Yoon, G.; Lim, K.; Kang, K. A comparative study of graphite electrodes using the co-intercalation phenomenon for rechargeable Li, Na and K batteries. *Chem. Commun.* **2016**, 52 (85), 12618–12621.
- (5) Dey, A.; Sullivan, B. The electrochemical decomposition of propylene carbonate on graphite. *J. Electrochem. Soc.* **1970**, 117 (2), 222.
- (6) Abe, T.; Kawabata, N.; Mizutani, Y.; Inaba, M.; Ogumi, Z. Correlation between co-intercalation of solvents and electrochemical intercalation of lithium into graphite in propylene carbonate solution. *J. Electrochem. Soc.* **2003**, *150* (3), A257.
- (7) Aurbach, D.; Zaban, A.; Ein-Eli, Y.; Weissman, I.; Chusid, O.; Markovsky, B.; Levi, M.; Levi, E.; Schechter, A.; Granot, E. Recent studies on the correlation between surface chemistry, morphology, three-dimensional structures and performance of Li and Li-C intercalation anodes in several important electrolyte systems. *J. Power Sources* 1997, 68 (1), 91–98.
- (8) Moon, H.; Tatara, R.; Mandai, T.; Ueno, K.; Yoshida, K.; Tachikawa, N.; Yasuda, T.; Dokko, K.; Watanabe, M. Mechanism of Li ion desolvation at the interface of graphite electrode and glyme—Li salt solvate ionic liquids. *J. Phys. Chem. C* **2014**, *118* (35), 20246—20256.
- (9) Asenbauer, J.; Eisenmann, T.; Kuenzel, M.; Kazzazi, A.; Chen, Z.; Bresser, D. The success story of graphite as a lithium-ion anode material—fundamentals, remaining challenges, and recent developments including silicon (oxide) composites. *Sustainable Energy & Fuels* **2020**, *4* (11), 5387–5416.
- (10) Liu, X.; Shen, X.; Li, H.; Li, P.; Luo, L.; Fan, H.; Feng, X.; Chen, W.; Ai, X.; Yang, H.; Cao, Y. Ethylene carbonate-free propylene carbonate-based electrolytes with excellent electrochemical compatibility for Li-ion batteries through engineering electrolyte solvation structure. *Adv. Energy Mater.* **2021**, *11* (19), 2003905.
- (11) Huang, Q.; Ma, L.; Liu, A.; Ma, X.; Li, J.; Wang, J.; Dahn, J. The reactivity of charged positive Li1-n [NixMnyCoz] O2 electrodes with electrolyte at elevated temperatures using accelerating rate calorimetry. *J. Power Sources* **2018**, *390*, 78–86.
- (12) Galushkin, N.; Yazvinskaya, N.; Galushkin, D. Mechanism of gases generation during lithium-ion batteries cycling. *J. Electrochem. Soc.* **2019**, *166* (6), A897.
- (13) Wang, C.; Xing, L.; Vatamanu, J.; Chen, Z.; Lan, G.; Li, W.; Xu, K. Overlooked electrolyte destabilization by manganese (II) in lithium-ion batteries. *Nat. Commun.* **2019**, *10* (1), 3423.
- (14) Yamada, Y.; Furukawa, K.; Sodeyama, K.; Kikuchi, K.; Yaegashi, M.; Tateyama, Y.; Yamada, A. Unusual stability of acetonitrile-based superconcentrated electrolytes for fast-charging lithium-ion batteries. *J. Am. Chem. Soc.* **2014**, *136* (13), 5039–5046.
- (15) Yamada, Y.; Usui, K.; Chiang, C. H.; Kikuchi, K.; Furukawa, K.; Yamada, A. General observation of lithium intercalation into graphite

- in ethylene-carbonate-free superconcentrated electrolytes. ACS Appl. Mater. Interfaces 2014, 6 (14), 10892–10899.
- (16) Lu, D.; Tao, J.; Yan, P.; Henderson, W. A.; Li, Q.; Shao, Y.; Helm, M. L.; Borodin, O.; Graff, G. L.; Polzin, B.; Wang, C.-M.; Engelhard, M.; Zhang, J.-G.; De Yoreo, J. J.; Liu, J.; Xiao, J. Formation of reversible solid electrolyte interface on graphite surface from concentrated electrolytes. *Nano Lett.* **2017**, *17* (3), 1602–1609.
- (17) Jiang, L. L.; Yan, C.; Yao, Y. X.; Cai, W.; Huang, J. Q.; Zhang, Q. Inhibiting Solvent Co-Intercalation in a Graphite Anode by a Localized High-Concentration Electrolyte in Fast-Charging Batteries. *Angew. Chem.* **2021**, *133* (7), 3444–3448.
- (18) Zeng, P.; Han, Y.; Duan, X.; Jia, G.; Huang, L.; Chen, Y. A stable graphite electrode in superconcentrated LiTFSI-DME/DOL electrolyte and its application in lithium-sulfur full battery. *Mater. Res. Bull.* **2017**, *95*, *61*–70.
- (19) Zeng, Z.; Murugesan, V.; Han, K. S.; Jiang, X.; Cao, Y.; Xiao, L.; Ai, X.; Yang, H.; Zhang, J.-G.; Sushko, M. L.; Liu, J. Non-flammable electrolytes with high salt-to-solvent ratios for Li-ion and Li-metal batteries. *Nature Energy* **2018**, *3* (8), 674–681.
- (20) Ming, J.; Cao, Z.; Wahyudi, W.; Li, M.; Kumar, P.; Wu, Y.; Hwang, J.-Y.; Hedhili, M. N.; Cavallo, L.; Sun, Y.-K.; Li, L.-J. New Insights on Graphite Anode Stability in Rechargeable Batteries: Li Ion Coordination Structures Prevail over Solid Electrolyte Interphases. *ACS Energy Letters* **2018**, 3 (2), 335–340.
- (21) Qian, K.; Winans, R. E.; Li, T. Insights into the Nanostructure, Solvation, and Dynamics of Liquid Electrolytes through Small-Angle X-Ray Scattering. *Adv. Energy Mater.* **2021**, *11* (4), 2002821.
- (22) Amine, R.; Liu, J.; Acznik, I.; Sheng, T.; Lota, K.; Sun, H.; Sun, C.-J.; Fic, K.; Zuo, X.; Ren, Y.; EI-Hady, D. A.; Alshitari, W.; Al-Bogami, A. S.; Chen, Z.; Amine, K.; Xu, G.-L. Regulating the Hidden Solvation-Ion-Exchange in Concentrated Electrolytes for Stable and Safe Lithium Metal Batteries. *Adv. Energy Mater.* **2020**, *10* (25), 2000901.
- (23) Holtstiege, F.; Schmuch, R.; Winter, M.; Brunklaus, G.; Placke, T. New insights into pre-lithiation kinetics of graphite anodes via nuclear magnetic resonance spectroscopy. *J. Power Sources* **2018**, 378, 522–526.
- (24) Kim, H.; Lim, K.; Yoon, G.; Park, J.-H.; Ku, K.; Lim, H.-D.; Sung, Y.-E.; Kang, K. Exploiting Lithium—Ether Co-Intercalation in Graphite for High-Power Lithium-Ion Batteries. *Adv. Energy Mater.* **2017**, *7* (19), 1700418.
- (25) Mohaček-Grošev, V.; Furić, K.; Ivanković, H. Observed bands in Raman and infrared spectra of 1, 3-dioxolane and their assignments. *Vib. Spectrosc.* **2013**, *64*, 101–107.
- (26) Seo, D. M.; Boyle, P. D.; Sommer, R. D.; Daubert, J. S.; Borodin, O.; Henderson, W. A. Solvate structures and spectroscopic characterization of LiTFSI electrolytes. *J. Phys. Chem. B* **2014**, *118* (47), 13601–13608.
- (27) Liu, X.; Fang, L.; Lyu, X.; Winans, R. E.; Li, T. Unveiling the Liquid Electrolyte Solvation Structure by Small Angle X-ray Scattering. *Chem. Mater.* **2023**, 35 (23), 9821–9832.
- (28) Liu, X.; Lee, S.-C.; Seifer, S.; Winans, R. E.; Cheng, L.; Z, Y; Li, T. Insight into the nanostructure of "water in salt" solutions: A SAXS/WAXS study on imide-based lithium salts aqueous solutions. *Energy Storage Materials* **2022**, *45*, 696–703.
- (29) Liu, X.; Lee, S.-C.; Seifert, S.; Winans, R. E.; Z, Y; Li, T. Relationship of the Molecular Structure and Transport Properties of Imide-Based Lithium Salts of "Acetonitrile/Water-in-Salt" Electrolytes. *Chem. Mater.* **2023**, 35 (16), 6415–6422.
- (30) Liu, X.; Lee, S.-C.; Seifert, S.; He, L.; Do, C.; Winans, R. E.; Kwon, G.; Z, Y; Li, T. Revealing the Correlation between the Solvation Structures and the Transport Properties of Water-in-Salt Electrolytes. *Chem. Mater.* **2023**, *35* (5), 2088–2094.
- (31) Lyu, X.; Wang, H.; Liu, X.; He, L.; Do, C.; Seifert, S.; Winans, R. E.; Cheng, L.; Li, T. Solvation Structure of Methanol-in-Salt Electrolyte Revealed by Small-Angle X-ray Scattering and Simulations. *ACS Nano* **2024**, *18* (9), 7037–7045.

- (32) Li, Y.; Lu, Y.; Adelhelm, P.; Titirici, M. M.; Hu, Y. S. Intercalation chemistry of graphite: alkali metal ions and beyond. *Chem. Soc. Rev.* **2019**, *48* (17), 4655–4687.
- (33) Liu, Y.; Lin, D.; Li, Y.; Chen, G.; Pei, A.; Nix, O.; Li, Y.; Cui, Y. Solubility-mediated sustained release enabling nitrate additive in carbonate electrolytes for stable lithium metal anode. *Nat. Commun.* **2018**, 9 (1), 3656.
- (34) Kouroupis-Agalou, K.; Liscio, A.; Treossi, E.; Ortolani, L.; Morandi, V.; Pugno, N. M.; Palermo, V. Fragmentation and exfoliation of 2-dimensional materials: a statistical approach. *Nanoscale* **2014**, *6* (11), 5926–5933.
- (35) Xia, Z. Y.; Pezzini, S.; Treossi, E.; Giambastiani, G.; Corticelli, F.; Morandi, V.; Zanelli, A.; Bellani, V.; Palermo, V. The exfoliation of graphene in liquids by electrochemical, chemical, and sonication-assisted techniques: A nanoscale study. *Adv. Funct. Mater.* **2013**, 23 (37), 4684–4693.
- (36) Li, Z.; Young, R. J.; Backes, C.; Zhao, W.; Zhang, X.; Zhukov, A. A.; Tillotson, E.; Conlan, A. P.; Ding, F.; Haigh, S. J.; Novoselov, K. S.; Coleman, J. N. Mechanisms of liquid-phase exfoliation for the production of graphene. *ACS Nano* **2020**, *14* (9), 10976–10985.
- (37) Du, W.; Jiang, X.; Zhu, L. From graphite to graphene: direct liquid-phase exfoliation of graphite to produce single- and few-layered pristine graphene. *Journal of Materials Chemistry A* **2013**, *1* (36), 10592–10606.
- (38) Nu Thanh Ton, N.; Ha, M.-Q.; Ikenaga, T.; Thakur, A.; Dam, H.-C.; Taniike, T. Solvent screening for efficient chemical exfoliation of graphite. 2D Materials 2021, 8 (1), No. 015019.
- (39) Hernandez, Y.; Nicolosi, V.; Lotya, M.; Blighe, F. M.; Sun, Z.; De, S.; McGovern, I. T.; Holland, B.; Byrne, M.; Gun'Ko, Y. K.; Boland, J. J.; Niraj, P.; Duesberg, G.; Krishnamurthy, S.; Goodhue, R.; Hutchison, J.; Scardaci, V.; Ferrari, A. C.; Coleman, J. N. High-yield production of graphene by liquid-phase exfoliation of graphite. *Nat. Nanotechnol.* **2008**, *3* (9), 563–568.
- (40) Coleman, J. N. Liquid exfoliation of defect-free graphene. Acc. Chem. Res. 2013, 46 (1), 14-22.
- (41) Cai, W.; Yao, Y.-X.; Zhu, G.-L.; Yan, C.; Jiang, L.-L.; He, C.; Huang, J.-Q.; Zhang, Q. A review on energy chemistry of fast-charging anodes. *Chem. Soc. Rev.* **2020**, *49*, 3806–3833.
- (42) Holoubek, J.; Kim, K.; Yin, Y.; Wu, Z.; Liu, H.; Li, M.; Chen, A.; Gao, H.; Cai, G.; Pascal, T. A.; Liu, P.; Chen, Z. Electrolyte design implications of ion-pairing in low-temperature Li metal batteries. *Energy Environ. Sci.* 2022, 15, 1647–1658.
- (43) Adams, R. A.; Varma, A.; Pol, V. G. Temperature dependent electrochemical performance of graphite anodes for K-ion and Li-ion batteries. *J. Power Sources* **2019**, *410*–*411*, 124–131.
- (44) See, K. A.; Lumley, M. A.; Stucky, G. D.; Grey, C. P.; Seshadri, R. Reversible capacity of conductive carbon additives at low potentials: caveats for testing alternative anode materials for Li-Ion batteries. *J. Electrochem. Soc.* **2017**, *164* (2), A327.
- (45) Billaud, J.; Bouville, F.; Magrini, T.; Villevieille, C.; Studart, A. R. Magnetically aligned graphite electrodes for high-rate performance Li-ion batteries. *Nature Energy* **2016**, *1*, 16097.
- (46) Zhang, X. Q.; Chen, X.; Cheng, X. B.; Li, B. Q.; Shen, X.; Yan, C.; Huang, J. Q.; Zhang, Q. Highly Stable Lithium Metal Batteries Enabled by Regulating the Solvation of Lithium Ions in Nonaqueous Electrolytes. *Angew. Chem., Int. Ed. Engl.* **2018**, *57* (19), 5301–5305.
- (47) Yu, Y.; Liu, Y.; Xie, J. Building Better Li Metal Anodes in Liquid Electrolyte: Challenges and Progress. ACS Appl. Mater. Interfaces 2021, 13 (1), 18–33.
- (48) Yu, Y.; Koh, H.; Zhang, Z.; Yang, Z.; Alexandrova, A. N.; Agarwal, M.; Stach, E. A.; Xie, J. Kinetic pathways of fast lithium transport in solid electrolyte interphases with discrete inorganic components. *Energy Environ. Sci.* 2023, 16 (12), 5904–5915.
- (49) Yan, C.; Yao, Y. X.; Chen, X.; Cheng, X. B.; Zhang, X. Q.; Huang, J. Q.; Zhang, Q. Lithium nitrate solvation chemistry in carbonate electrolyte sustains high-voltage lithium metal batteries. *Angew. Chem.* **2018**, *130* (43), 14251–14255.

- (50) Fu, J.; Ji, X.; Chen, J.; Chen, L.; Fan, X.; Mu, D.; Wang, C. Lithium nitrate regulated sulfone electrolytes for lithium metal batteries. *Angew. Chem.* **2020**, *132* (49), 22378–22385.
- (51) Li, T.; Zhang, X.-Q.; Shi, P.; Zhang, Q. Fluorinated Solid-Electrolyte Interphase in High-Voltage Lithium Metal Batteries. *Joule* **2019**, 3 (11), 2647–2661.
- (52) Suo, L.; Xue, W.; Gobet, M.; Greenbaum, S. G.; Wang, C.; Chen, Y.; Yang, W.; Li, Y.; Li, J. Fluorine-donating electrolytes enable highly reversible 5-V-class Li metal batteries. *Proc. Natl. Acad. Sci. U. S. A.* 2018, *115* (6), 1156–1161.
- (53) Fan, X.; Chen, L.; Borodin, O.; Ji, X.; Chen, J.; Hou, S.; Deng, T.; Zheng, J.; Yang, C.; Liou, S.-C.; Amine, K.; Xu, K.; Wang, C. Non-flammable electrolyte enables Li-metal batteries with aggressive cathode chemistries. *Nat. Nanotechnol.* **2018**, *13* (8), 715–722.
- (54) Lu, Y.; Tu, Z.; Archer, L. A. Stable lithium electrodeposition in liquid and nanoporous solid electrolytes. *Nat. Mater.* **2014**, *13* (10), 961–969.
- (55) Efaw, C. M.; Wu, Q.; Gao, N.; Zhang, Y.; Zhu, H.; Gering, K.; Hurley, M. F.; Xiong, H.; Hu, E.; Cao, X.; Xu, W.; Zhang, J.-G.; Dufek, E. J.; Xiao, J.; Yang, X.-Q.; Liu, J.; Qi, Y.; Li, B. Localized high-concentration electrolytes get more localized through micelle-like structures. *Nat. Mater.* 2023, 22, 1531–1539.